



Mechanical Behavior of Slender Composite Columns under Axial Compression Load

Nwzad Abduljabar Abdulla¹

¹Dept. of Civil Engineering, College of Engineering, Salahaddin University, Erbil, Iraq

ARTICLE HISTORY

Received 17 April 2019
Revised 21 August 2019
Accepted 28 October 2019
Published Online 4 December 2019

KEYWORDS

Steel cage
Rebar
Plastic form
Composite column
Ductility index
B/A ratio

ABSTRACT

In the present experimental investigation, polyvinyl chloride (PVC) plastic pour-in form (PPF) was used in three low-cost composite systems for concrete construction. It included concrete-filled tubular plastic forms (CPPF), steel-reinforced concrete-filled tubular plastic (CPPF-SC and CPPF-Re), and welded wire fabric reinforced concrete-filled tubular plastic (CPPF-WM). The core was laboratory mixed concrete with an average 28-day compressive strength of 31.3 MPa. The performance of the three systems was compared with the corresponding pure concrete (PC), and reinforced concrete (RC) specimens, by testing 16 slender specimens with unequal end restraint-conditions. The analyzed parameters were the tube thickness and diameter, the amount and yield strength of longitudinal reinforcement, slenderness ratio and the rotation of the upper loading steel platen. The test results show that using PPF a hinge was formed and the mode of failure changed from brittle shear for RC specimens to ductile beam failure mode for CPPF with compression softening. The extent of enhancement in strength and ductility depends on the type of composite specimen.

1. Introduction

The inelastic behavior of concrete compression members has significant influence on the overall performance of concrete structures. Several materials have been investigated for such purpose; steel tie (Sheikh and Uzumeri, 1982), steel fiber with the nominal tie (Lima Junior and Giongo, 2004), steel tube (Xiamuxi and Hasegawa, 2011) and FRP grids (Ding et al., 2011). Another material with the potential to increase the strength and improve the ductility of concrete columns is the thermoplastic PPF with large deformations before the ultimate failure. PVC is a thermoplastic polymer with repeated molecule chains changeable for the better, expanding product possibilities and facilitating its recycling. Intermolecular attractions between atoms result in improved overall stiffness, tensile strength and modulus compared to other plastics (Pan et al., 2004). Field tests have shown that it has good durability with satisfactory protection from deterioration and weathering (Merah et al., 2013). The Poly vinyl chloride (PVC) not only provides the form for the concrete and steel reinforcement but also resists the axial load and contains the lateral expansion of concrete core. Compared with steel tube of similar thickness, its density is nearly 1/6 of steel

tube and can be considered as a lightweight material (Abdulla, 2017). The yield strength and elastic modulus of plastic tube are nearly 1/6 and 1/50 of that for steel tube, 248 MPa and 191GPa. The thermal conductivity of PPF is only 0.6% of that of steel which is important to reduce the hydration heat of concrete core. Protection of the concrete and mitigating the corrosion of conventional reinforcement found in concrete located in hostile environments has been a major challenge to the design engineer. Piles found in aggressive environments, splash zone, are vulnerable to corrosion (Stapleman, 1997).

With its excellent anti-corrosion characteristics, the tubular plastic can act as a barrier and protect compression members found in the splash/tidal zone or in contact with soil from corrosion (Fujiwara et al., 1992). The polymeric tube is produced in sizes enough to confine bridge piers and is of remarkable versatility, making it suitable for civil and construction applications with high potential to replace the steel mold in column construction resulting in lower costs and shorter durations of casting. Previous studies were mostly performed on short CPPF specimens' subjected to uniaxial load (Abdulla, 2014; Oyawa et al., 2016). Unlike FRP, which features a brittle failure, the PPF has low stiffness but higher elongation at break which can mitigate the

CORRESPONDENCE Nwzad Abduljabar Abdulla ✉ anwzad@yahoo.com 📧 Dept. of Civil Engineering, College of Engineering, Salahaddin University, Erbil, Iraq

© 2020 Korean Society of Civil Engineers

bad ductility and brittle failure of concrete (Fakharifar and Chen, 2016). The strength of unconfined concrete was increased by 2 folds and steel reinforcement inclusion was of no significance in short stub specimens (Maiturare, 1990). Chen et al. (2016) evaluated the structural behavior of steel–concrete–PVC SHS joints under axial compression load. The joints had PVC tube and SHS steel tubes as the inner and outer tubes of chord member. PVC structural angles were employed to enhance the capacity of reinforced concrete beams (Naish et al., 2013). The PPF can reduce damages due to impact and vandalism associated with FRP tubes, where the former is more flexible and the fiber could be applied any time after casting concrete.

The use of PPF was stretched to field studies where a 592-mm diameter and 18 m long PPF-concrete composite pile was tested (United States Department of Transportation, 2006) for bridge substructures. Other potential uses include piers and bridges columns in aggressive environments. The lightly reinforced PPF can find applications in light structural constructions, such as industrial buildings and small residential buildings (Abdulla, 2019). Generally, there is no study on the load performance of slender CPPF with the inclusion of steel cages, bars or wire meshes. The objective of the current experimental work was to ascertain the influence of the polymeric tube on the mechanical properties of steel-reinforced concrete. The development of a consistent set of laboratory experimental results together with simple analytical expressions to aid in assessing the behavior of CPPF under load will be a notable and simple technique comparable to the existing state-of-the-art techniques.

2. Experimental Investigation

2.1 Materials Details

Two groups of specimens, A and B, were prepared and cast and the concrete mix details were summarized in Table 1. The mechanical properties of the PPF which included the yield strength, compressive strength ($f_{p,w}$), and the elastic modulus (E_p) were determined from coupon and tube tests, typical compression failure of coupon and PPF is shown in Fig. 1. For the slender specimen casting, tubes were cut to the required height and used as temporary and stay-in-place formworks. All specimen details of groups A and B were shown in Tables 2 and 3, respectively.

Table 1. Mix Details of Groups A and B Concrete

| Material properties | |
|-------------------------------|-------------|
| Water | 160 Kg |
| Cement: (SG = 3.15) | 360 Kg |
| Sand: (SG = 2.6) | 630 Kg |
| Coarse aggregate: (SG = 2.65) | 1260 Kg |
| w/c ratio | 0.5 |
| Maximum aggregate size | 9.5 mm |
| Slump | 100 ± 10 mm |
| Average compressive strength | 31.3 MPa |

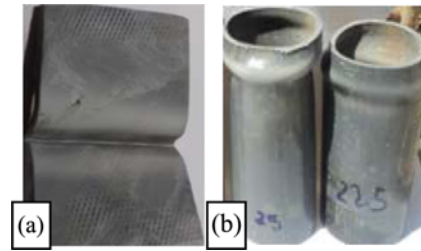


Fig. 1. Typical Compression Failure of: (a) Coupon, (b) PPF

Table 2. Specimen Details of Group A

| No. | L mm | D mm | $0.8l_w/$ $0.25D$ | Reinf. type |
|------|-----------|-----------|----------------------|----------------|
| A1-1 | 900 | 67 | 43 | - |
| A1-2 | 1,000 | 67 | 47.8 | - |
| A1-3 | 1,200 | 100 | 38.4 | I |
| A1-4 | 1,000 | 100 | 32 | I |
| A1-5 | 1,100 | 81 | 43.5 | - |
| A1-6 | 1,100 | 100 | 35.2 | I |
| A1-7 | 850 | 67 | 4.6 | - |
| A1-8 | 1,200 | 100 | 38.4 | II |

Table 3. Specimen Details of Group B

| No. | L mm | D mm | t_p | $0.8l_w/$ $0.25D$ | Reinf. Type | Reinf. system |
|------|-----------|-----------|-------|----------------------|----------------|------------------|
| B2-1 | 1,200 | 110 | 5 | 35 | II | CPPF-SC |
| B2-2 | 1,200 | 100 | - | 38.4 | - | PC |
| B2-3 | 1,100 | 100 | - | 35.2 | - | PC |
| B2-4 | 1,000 | 75 | 4 | 42.7 | - | CPPF |
| B2-5 | 1,100 | 75 | 4 | 47 | III | CPPF-Re |
| B2-6 | 1,100 | 110 | 5 | 32 | IV | CPPF-WM |
| B2-7 | 1,000 | 75 | - | 47 | III | C-Re |
| B2-8 | 1,100 | 100 | - | 35.2 | IV | C-WM |



Fig. 2. Details of Type I Steel Cages

Types of reinforcement included steel cages, Fig. 2, longitudinal steel bars (1 or 2 bars) in the center of the section, and household wire mesh (WM). Reinforcement details of the two groups A and B were given in Tables 4 and 5, respectively. Group A was a

Table 4. Reinforcement Details of Group A







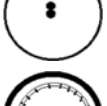
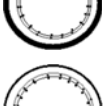
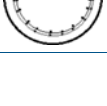
| Steel reinforcement | | | | |
|---------------------|---|---|---------------------------|---|
| Type | Main steel | Steel Tie | Group | Cross-section |
| SC-I | 6 ϕ 8 mm plain $0.01 < (\rho_{s,PL} = 0.0384) < 0.08$ $f_y = 250$ MPa | ϕ 6 mm deformed @100 mm ^c / _c $f_y = 250$ MPa | One: A1-3 A1-4 A1-6 |  |
| SC-II | 6 ϕ 6 mm deformed; $0.01 < (\rho_s = 0.01785) < 0.08$ $f_y = 460$ MPa | ϕ 2.5 mm deformed @96 mm ^c / _c $f_y = 460$ MPa | One: A1-8 |  |

Table 5. Reinforcement Details of Group B

| Steel reinforcement | | | | |
|---------------------|---|--|--------|---|
| Reinf. system | Main steel | Steel Tie | Column | |
| CPPF-SC Type II | 6 ϕ 6 mm deformed; $0.01 < (\rho_s = 0.01785) < 0.08$ $f_y = 460$ MPa | ϕ 2.5 mm deformed @96 mm ^c / _c $f_y = 460$ MPa | B2-1 |  |
| CPPF | 1 ϕ 6 mm deformed; $(\rho_s = 0.0064) < 0.01$ $f_y = 460$ MPa | - | B2-4 |  |
| - | 1 ϕ 6 mm deformed; $(\rho_s = 0.0064) < 0.01$ $f_y = 460$ MPa | - | A-app |  |
| CPPF-Re Type III | 2 ϕ 6 mm deformed; $0.01 < (\rho_s = 0.0128) < 0.08$ $f_y = 460$ MPa | - | B2-5 |  |
| C-Re Type III | 2 ϕ 6 mm deformed; $0.01 < (\rho_s = 0.0128) < 0.08$ $f_y = 460$ MPa | - | B2-7 |  |
| CPPF-WM Type IV | WM; 25 by 25 mm galvanized 1 mm wire; two rounds $f_y = 240$ MPa | - | B2-6 |  |
| C-WM Type IV | WM; 25 by 25 mm galvanized 1 mm wire; two rounds, $f_y = 240$ MPa | - | B2-8 |  |

comparative group with four pure concrete specimens PC and four RC columns, Table 2. Group B was the main group with the three reinforcement systems; CPPF-SC (B2-1) and CPPF-Re (B2-5), CPPF (B2-4), and CPPF-WM (B2-6), Table 3, in addition to two PC and one RC and WM specimens.

The prefabricated WM had steel wires running in two orthogonal directions and welded at the intersections. One of the alternatives to conventional reinforcement is WM which yields easier and faster construction and eliminates some of the detailing problems associated with conventional steel reinforcement. Light household WM is a new technique that needs investigation for its performance in concrete elements for ductility enhancement. Concrete compression member must contain minimum amount of longitudinal reinforcement. However, column B2-4 had

longitudinal steel ratio ($\rho_s = 0.64\%$) less than the minimum amount (1%) mandated by ACI 318R-014 (2014). Therefore it's classified as a plain or unreinforced concrete column, Tables 4 and 5. In addition, column B2-4 was encased in PPF and it formed the type CPPF of the reinforcement system. The models for the three reinforcement systems; CPPF (unreinforced), CPPF-Re and CPPF-SC (reinforced with 2 rebars, Re, or steel cage, SC), and CPPF-WM (reinforced with WM) are shown in (Figs. 3(a) – 3(d)).

2.2 Specimens Casting

The plastic forms were placed vertically inside horizontal timber formworks resting on a large horizontal vibrating table ready for casting. The specimens were compacted in three layers and the concrete cover was 20 mm thick at top and bottom, and 12.5 mm

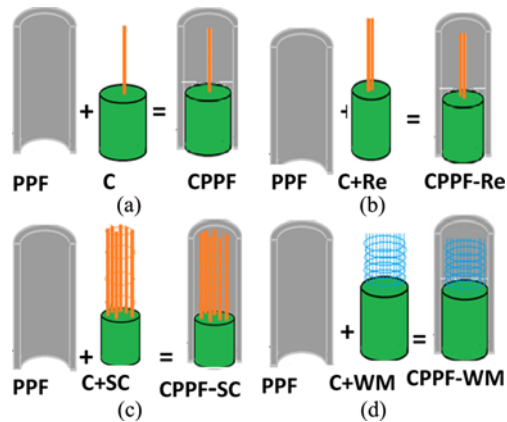


Fig. 3. Models of the Reinforcement Systems: (a) CPPF, (b) CPPF-Re, (c) CPPF-SC, (d) CPPF-WM

on the circular surface. At least three concrete cylinder specimens (100 mm in diameter and 200 mm in length) were cast from each concrete batches. After casting, specimens were covered with wet burlaps and moist cured for 28 days.

3. Test Procedure and Results

The specimens were placed vertically to be tested for different end-restraint conditions, hinged at top and restrained at the bottom by a stiff steel plate (which was considered as fixed). Four LVDTs at the mid-height were used to monitor the deflections. The slender columns were tested in a testing machine with a load capacity of 400 KN. To monitor the swiveling head rotations, two inclinometers were mounted horizontally on top of it, in two orthogonal directions. The schematic of the test set-up is shown in Fig. 4. The average concrete strength was measured to be 31.3 MPa for the two groups.

3.1 Failure modes

When concrete was not confined or reinforced the post-peak

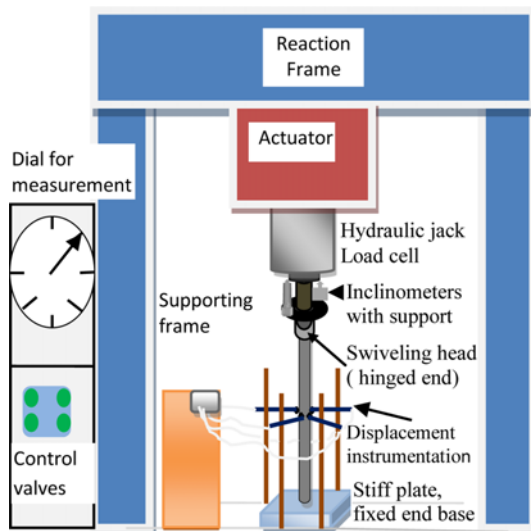


Fig. 4. Test Set Up

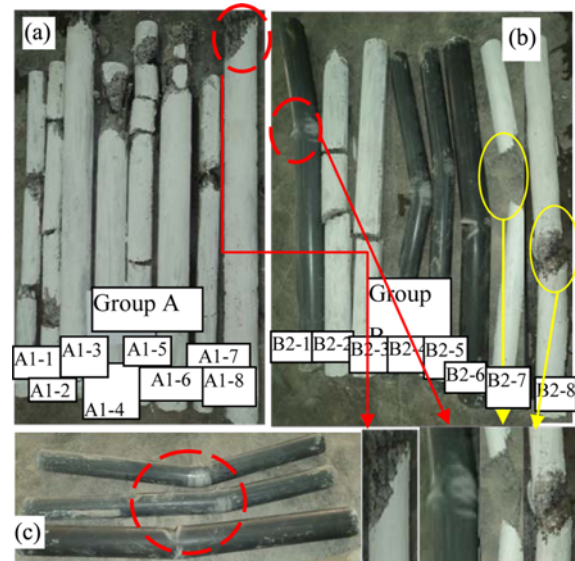


Fig. 5. Typical Failure of Columns: (a) Group A, (b) Group B, (c) CPPF (the developed deflected shapes)

failure was sudden explosive with negligible deformations (due to the low flexural ductility and shear strength) as was the case for pure concrete columns A1-1, A1-2, A1-5, and A1-7 (ruptured into 3, 4, 5 and 3 parts, respectively) depending on the slenderness ratio, Fig. 5(a), and B2-2, B2-3 (which were ruptured into 3 and 2 parts, respectively) Fig. 5(b). The RC specimens A1-3, A1-4, A1-6, and A1-8, exhibited a completely different behavior. The concrete in the zone close to the top end bearing plate suffered bursting and splitting produced by the high concentrated stresses and these locations were approximated to be one to three cross-section depths from top of the column. The depth of failure sections of the three systems was located near the mid-height. In CPPF-Re and CPPF-SC the failure mode was initiated by tension-steel yielding, crushing of the concrete and finally buckling of the plastic tube. However, in CPPF failure was initiated by crushing of the concrete and consequently the yield and buckling of the plastic tube. The extra capacity of CPPF-Re and CPPF-SC might be due to the delayed yielding of the plastic tube in the presence of tension steel (Abdel Havez, 2014) and the possible strain hardening of steel. The post-peak behavior for CPPF-SC was characterized with a less steep drop and higher ductility performance, indicating wider post-peak curves than its counterpart, column A1-8. The failure of CPPF composite columns was due to the yield of the PPF on tension side and the subsequent strain hardening, which manifested itself in terms of a fine white patch, and the local buckling due to loss of tangential surface contacts on the compression side, Fig. 5(c). The CPPF (B2-4), which was reinforced with one 6 mm steel bar, showed enhanced performance compared to the member reinforced with two 6 mm bars (B2-7) which failed with spalling and crushing in the proximity of the collapse zone, Fig. 5(b). Failure of C-WM was due buckling and the breaking of wire mesh at welded joint along the critical section. CPPF-WM displayed a similar failure mechanism but

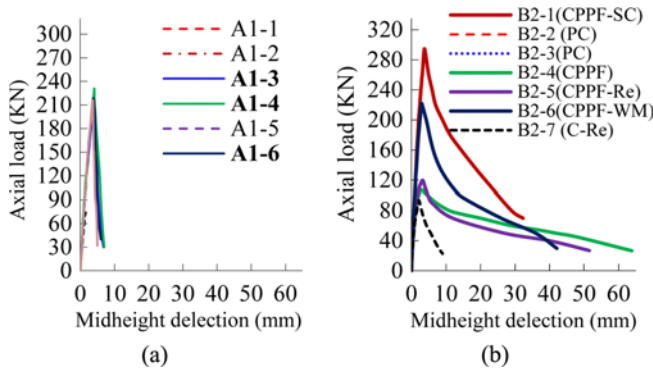


Fig. 6. Load-Deflection Diagrams: (a) Group A, (b) Group B

with a clear single curvature, Fig. 5(b).

3.2 Deflection

The P - Δ curves, Figs. 6(a) and 6(b), had a linear elastic branch till a load of about 0.6 – 0.7, 0.5 – 0.8, and 0.7 – 0.8 for PC, RC, and CPPF specimens. The polymeric tube influenced the descending branch of the load-deformation curve for the low modulus CPPF composite system. The maximum sustainable lateral displacement increased by more than 27 times from approximately 2.3 mm for pure concrete specimens (A1-2) to 63.8 mm for the corresponding CPPF, (B2-4). Such trend enhanced the absorbed energy capacity and manifested itself by the area under the load-deflection curve. Pure concrete specimens showed very small lateral deformation with no descending branch. The presence of steel reinforcement resulted in additional improvement in the post-peak deformation capacity with the additional area under the load-deflection curves.

3.3 Mechanism of Plastic Tube Confinement

The plastic tube with its circular cross-section developed a uniform lateral pressure which resisted the lateral dilation of concrete core to some extent. At low stresses the tube resistance to concrete dilation was initiated, thereby offering passive resistance to concrete expansion. At later stages, induced stresses from the increased load minimized the tube confining mechanism. The composite system failed at the ultimate load as a result of excessive expansion of concrete core due to yielding of the plastic tube. In FRP-confined specimens, a limit has been set on the ratio of $f_{rmp}/f_{oc} = 0.08$ in order to ensure strength enhancement, ACI 440.2R-08 (2008). Strength enhancements below this limit signify low confinement which may be applied to the plastic tube to some extent.

4. Test Parameters

4.1 Specimen Geometry

The effective slenderness ratio kL/r was used to classify the specimens as short ≤ 22 or slender > 22 (ACI 318-14), where l_u = unbraced length of the column; k = effective length factor for the compression member; and r = radius of gyration. For the pinned-

fixed end conditions, the k value was approximated to 0.8. Based on this value ($0.8l_u/0.25D = 22$) the $L/D = 6.8$ was the limit for a short column in a non-sway frame. All the columns were sensitive to the change in the slenderness ratio. The experimental results showed that hinged-end restraint condition adversely affected the load capacity of the columns while increasing their ductility.

4.2 Strain Softening

Pure concrete columns had no post-peak response. Due to the flexibility effect offered by the plastic tube, CPPF specimens experienced post-peak softening behavior as the load was dropped down and this behavior continued until the load reached 25% of the ultimate load without any rupture or crack and the test had to be stopped to prevent any damage to measuring instrumentation due to the excessive rotation of the swiveling head.

4.3 Ratio and Yield Strength of Longitudinal Steel

Higher yield strength longitudinal bars can delay the transfer of lateral pressure to the steel ties, resulting in improved behavior. RC specimen (A1-8) had similar slenderness (38) to A1-3 but lower steel ratio ($\rho_s = 0.0178$), approximately half of that for A1-3 (0.0384) and yielded higher strength capacity, 216 KN compared with 212 for A1-3, however, its failure was less ductile. Steel ties restrain the lateral buckling of longitudinal steel. Improved post-peak behavior of more than 20% was observed for specimens reinforced with longitudinal steel having yield strength of 250 MPa compared with its equivalent reinforced specimens with yield strength of 460 MPa. This could be ascribed to the stiffer ties used in the former ($\phi 6$ mm deformed bar) compared with ($\phi 2.5$ mm deformed bar) for the latter.

4.4 Plastic Tube

The PPF eliminated the sudden loss of column strength due to unstable cover. The plastic tube resisted the gravity load and sustained the inelastic deformations to maintain compatibility with the concrete core. As a result, the concrete strength, column ductility, and rigidity were improved. The influence of the PPF on enhancing the post-peak behavior was more significant for specimens having a small steel ratio.

4.5 Plastic Rotation

The RC specimens showed lower rotation capacity and were largely influenced by the swiveling head which resulted in most cases in brittle pre-mature shear failure. Slender CPPF yielded favorable plastic deformation under axial compression by enhancing the column's rotational capacity and allowing the specimens to resist axial loads with increasing lateral displacements. These failure modes for CPPF are desirable in practice since it contains the deformation, crack, and lateral dilation of concrete. CPPF may reach a state where a hinge is formed at the critical section due to excessive yielding. The location of the critical section for the ultimate load was located near the mid-height of column. At

Table 6. The B/A Ratio for Specimens of Groups A and B

| No. | Load-deflection curve | | | | A | B | B/A |
|------|-----------------------|--------------------|------------------------|-------------------------|--------|--------|-------|
| | L (mm) | Δ_y (mm) | $\Delta_{0.8}$ (mm) | $\Delta_{0.25}$ (mm) | | | |
| A1-1 | 900 | 1.00 | 2.15 | 2.15 | 0.0002 | 0.0002 | 1.00 |
| A1-2 | 1,000 | 0.80 | 2.30 | 2.30 | 0.0001 | 0.0001 | 1.00 |
| A1-3 | 1,200 | 3.30 | 4.78 | 6.00 | 0.0012 | 0.0023 | 1.92 |
| A1-4 | 1,000 | 3.40 | 4.60 | 6.45 | 0.0012 | 0.0031 | 2.54 |
| A1-5 | 1,100 | 1.25 | 2.15 | 2.15 | 0.0001 | 0.0001 | 1.00 |
| A1-6 | 1,100 | 3.20 | 4.45 | 5.50 | 0.0011 | 0.0021 | 1.91 |
| A1-7 | 850 | 1.40 | 2.16 | 2.16 | 0.0002 | 0.0002 | 1.00 |
| A1-8 | 1,200 | 3.20 | 4.53 | 5.25 | 0.0011 | 0.0017 | 1.55 |
| B2-1 | 1,200 | 3.01 | 6.60 | 30.0 | 0.0030 | 0.0225 | 7.5 |
| B2-2 | 1,200 | 1.39 | 2.14 | 2.14 | 0.0001 | 0.0001 | 1.0 |
| B2-3 | 1,100 | 1.55 | 2.18 | 2.18 | 0.0002 | 0.0002 | 1.0 |
| B2-4 | 1,000 | 1.65 | 9.00 | 63.8 | 0.0073 | 0.0062 | 8.5 |
| B2-5 | 1,100 | 1.69 | 7.90 | 49.0 | 0.0062 | 0.0471 | 7.6 |
| B2-6 | 1,100 | 1.67 | 5.50 | 34.5 | 0.0035 | 0.0298 | 8.5 |
| B2-7 | 1,000 | 1.50 | 3.30 | 9.00 | 0.0018 | 0.0075 | 4.26 |
| B2-8 | 1,100 | 1.50 | 2.25 | 2.42 | 0.0007 | 0.0008 | 1.14 |

| No. | Load-rotation curve | | | | A | B | B/A |
|------|---------------------|--------------------------------|------------------------------------|-------------------------------------|--------|--------|-------|
| | D (mm) | θ_y (rad 10^{-2}) | $\theta_{0.8}$ (rad 10^{-2}) | $\theta_{0.25}$ (rad 10^{-2}) | | | |
| A1-1 | 67 | 0.59 | 0.65 | 0.65 | 0.0001 | 0.0001 | 1.0 |
| A1-2 | 67 | 0.47 | 0.51 | 0.51 | 0.0001 | 0.0001 | 1.0 |
| A1-3 | 100 | 1.63 | 2.38 | 3.0 | 0.0006 | 0.0011 | 1.83 |
| A1-4 | 100 | 1.68 | 2.60 | 3.35 | 0.0009 | 0.0017 | 1.88 |
| A1-5 | 81 | 0.73 | 0.78 | 0.78 | 0.0001 | 0.0001 | 1.0 |
| A1-6 | 100 | 1.70 | 2.30 | 2.67 | 0.0005 | 0.0009 | 1.80 |
| A1-7 | 67 | 0.60 | 0.67 | 0.67 | 0.0006 | 0.0006 | 1.0 |
| A1-8 | 100 | 1.80 | 2.25 | 2.63 | 0.0004 | 0.0006 | 1.72 |
| B2-1 | 110 | 2.0 | 4.0 | 14.7 | 0.0016 | 0.0110 | 6.9 |
| B2-2 | 100 | 1.36 | 1.40 | 1.40 | 0.0001 | 0.0001 | 1 |
| B2-3 | 100 | 1.24 | 1.35 | 1.35 | 0.0001 | 0.0001 | 1 |
| B2-4 | 75 | 1.33 | 3.50 | 16.3 | 0.0018 | 0.0150 | 8.30 |
| B2-5 | 75 | 1.36 | 3.10 | 13.9 | 0.0017 | 0.0125 | 7.35 |
| B2-6 | 110 | 1.85 | 3.50 | 13.0 | 0.0015 | 0.0103 | 6.67 |
| B2-7 | 75 | 1.37 | 2.20 | 4.40 | 0.0008 | 0.0030 | 3.75 |
| B2-8 | 100 | 1.35 | 2.05 | 2.33 | 0.0006 | 0.0009 | 1.5 |

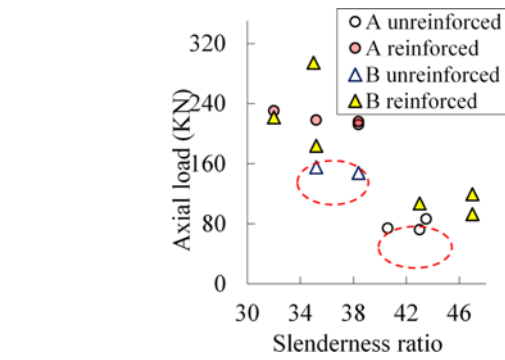
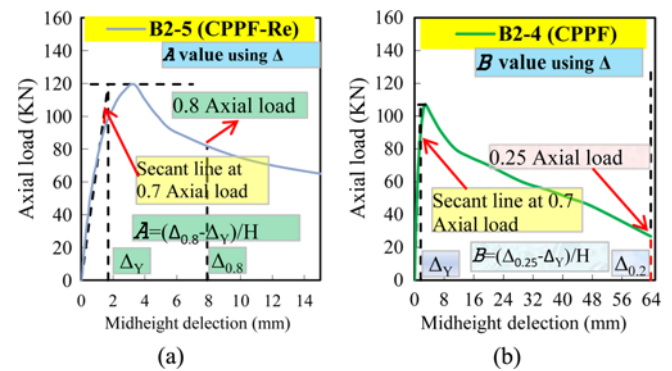
maximum load, the curvature and strains were concentrated in the critical section and appeared as a hinge (lines of white patches) as shown in Fig. 5(c).

4.6 The B/A Ratio

The B/A ratios were used to express the plastic rotation capacity of the columns (ASCE/SEI-41, 2007), Table 6, using two approaches:

1. From load-deflection diagram ($P-\Delta$); A was estimated as follows:

$$A = (\Delta_{0.8} - \Delta_y)/H \quad (1)$$


Fig. 7. Axial Load Versus Slenderness Ratio for Groups A and B

Fig. 8. Axial Load-Deflection Diagrams for Evaluating the Value of: (a) A , (b) B

Where,

A = plastic rotations (the degree of inelastic deformations)

H = column clear height.

$\Delta_{0.8}$ = post-peak deflection corresponding to 20% of strength degradation

Δ_y = deflection at onset of yield

A secant line was stretched on the load-deflection diagram from the origin to the point on the curve at 70% of the maximum load (Sezen and Moehle, 2004; Ghannoum and Matamoros, 2014), Figs. 8(a) and 8(b). The Δ_y represented the deflection at yield point, the intersection of the secant line with the horizontal line drawn at maximum load (Ghannoum and Matamoros, 2014). B = plastic rotation at 75% of the strength degradation of the peak load and was calculated as follows:

$$B = (\Delta_{0.25} - \Delta_y)/H \quad (2)$$

where $\Delta_{0.25}$ was deflection at onset of collapse.

2. From load-rotation diagram ($P-\theta$), A was estimated as follows:

$$A = (\theta_{0.8} - \theta_y)/H \quad (3)$$

Where,

$\theta_{0.8}$ = post-peak rotation corresponding to 20% of strength degradation

θ_y = rotation at onset of yield

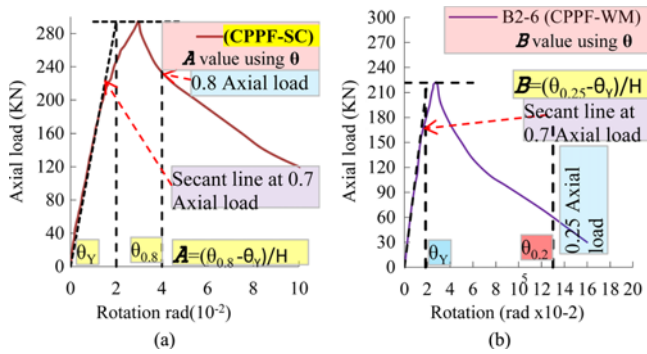


Fig. 9. Axial Load-Rotation Diagrams for Evaluating the Value of: (a) A, (b) B

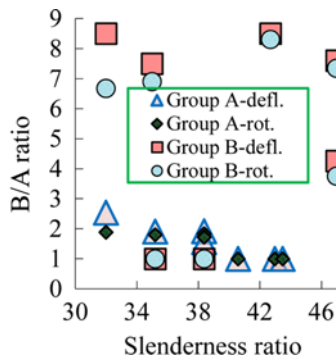


Fig. 10. The B/A Ratio versus Slenderness Ratio

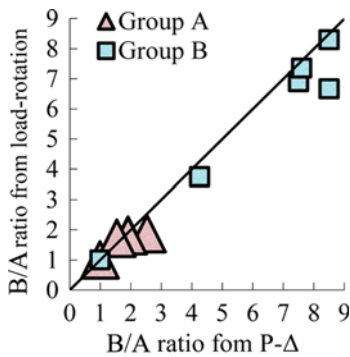


Fig. 11. The B/A Ratios from P-θ and P-Δ

A secant line was stretched on the load-rotation diagram from the origin to the point on the curve at 70% of the maximum load, Figs. 9(a) and 9(b). θ_Y was taken as the rotation at the intersection of the secant line with the horizontal line drawn at maximum load.

B was calculated as follows:

$$B = (\theta_{0.25} - \theta_Y)/H \tag{4}$$

where $\theta_{0.25}$ was the rotation at onset of the collapse. The CPPF specimens showed the highest B/A ratio (7.5 to 8.5) from load-deflection curve and (6.67 to 8.3) from load-rotation curve (Table 6), whereas RC specimens showed lower values (1.55 to 2.54) and (1.72 to 1.88) due to the lower rotation capacity. The rotation capacity of PC specimens was negligible, 1, and was ignored. The B/A ratio versus slenderness ratio for groups A and

B were plotted in Fig. 10. The correlation between B/A ratios calculated from P-θ and P-Δ diagrams shown in Fig. 11. A better correlation (more linear) was observed for group B compared with group A.

4.7 Ductility

When the confinement level is low, which is the case with the plastic tube, the deformations generated are termed softening strain. The displacement capacity of specimens was used to evaluate the ductility index. Ductility was increased with the decrease in slenderness ratio and an increase in the amount of longitudinal reinforcement and the use of PPF. The improvement in axial compression strength and ductility enabled the CPPF column to behave like a beam thereby increasing the flexural bending capacity of the column. For CPPF, it was noted that the effect of slenderness was more on ductility. Small enhancement in ductility was achieved using WM; it can withstand small lateral pressure from the concrete core due to its high slenderness, 1 mm diameter only. Some researchers have proposed deformations indexes based on section capacity and the behavior of the member under the load (Mufti et al., 1996). The indexes include strength and deformation parameters to reflect the overall performance. Two parameters, deflection, and rotation were used for the columns and one parameter for the section.

$$I_{S_A} = \frac{P_U}{P_Y} = \text{strength index} \tag{5}$$

$$I_{D_A} = \frac{\Delta_U}{\Delta_Y} = \text{deformation index} \tag{6}$$

$$I_{C_A} = I_{S_A} \cdot I_{D_A} \tag{7}$$

Where,

I_C = The column ductility index expressed by I_S and I_D

P_U = peak load

P_Y = yield load

Δ_Y and Δ_U = the deflections at the yield and peak load.

Similarly using the second parameter (rotation):

$$\text{Strength index} = I_{S_\theta} = \frac{P_U}{P_Y} \tag{8}$$

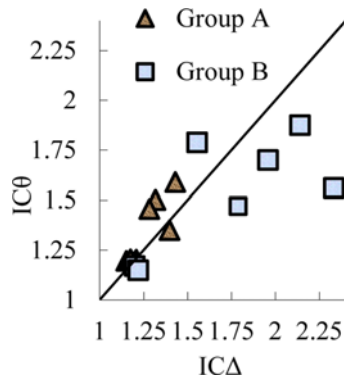
$$\text{Deformation index} = I_{D_\theta} = \frac{\theta_U}{\theta_Y} \tag{9}$$

$$I_{C_\theta} = I_{S_\theta} \cdot I_{D_\theta} \tag{10}$$

where θ_Y and θ_U : the rotations at the yield and peak. The computed results for ductility indexes using the two proposed Eqs. (7) and (10) were summarized in Table 7. With I_{C_d} and I_{C_r} values from 1.566 to 2.177 and 1.56 to 1.788 for group B (CPPF) specimens compared with 1.284 to 1.433 and 1.35 to 1.589 for group A. The three reinforcement systems showed better results for the two ductility indexes, compared with its equivalent RC and PC specimens. The ductility index from the load-deflection curve versus index calculated from load-rotation curve was

Table 7. Ductility Indexes for Columns Using $P-\Delta$ and $P-\theta$ Curves

| No. | Load-deflection curve | | | | | | |
|------|-----------------------|---------------|---------------|---------------|---------------|---------------|---------------|
| | $0.8I_u/0.25D$ | $I_{D\Delta}$ | $I_{S\Delta}$ | $I_{C\Delta}$ | $I_{D\theta}$ | $I_{S\theta}$ | $I_{C\theta}$ |
| A1-1 | 43 | 1.150 | 1.075 | 1.236 | 1.091 | 1.101 | 1.201 |
| A1-2 | 47.8 | 1.112 | 1.076 | 1.200 | 1.097 | 1.085 | 1.190 |
| A1-3 | 38.4 | 1.234 | 1.134 | 1.399 | 1.168 | 1.157 | 1.350 |
| A1-4 | 32 | 1.244 | 1.152 | 1.433 | 1.410 | 1.393 | 1.589 |
| A1-5 | 43.5 | 1.080 | 1.068 | 1.153 | 1.119 | 1.068 | 1.195 |
| A1-6 | 35.2 | 1.098 | 1.203 | 1.32 | 1.191 | 1.260 | 1.501 |
| A1-7 | 40.6 | 1.114 | 1.057 | 1.177 | 1.079 | 1.116 | 1.204 |
| A1-8 | 38.4 | 1.156 | 1.111 | 1.284 | 1.207 | 1.206 | 1.455 |
| B2-1 | 35 | 1.269 | 1.226 | 1.556 | 1.490 | 1.20 | 1.788 |
| B2-2 | 38.4 | 1.180 | 1.083 | 1.200 | 1.137 | 1.029 | 1.170 |
| B2-3 | 35.2 | 1.123 | 1.087 | 1.220 | 1.093 | 1.050 | 1.148 |
| B2-4 | 42.7 | 1.776 | 1.103 | 1.959 | 1.429 | 1.189 | 1.699 |
| B2-5 | 47 | 1.953 | 1.195 | 2.334 | 1.375 | 1.138 | 1.560 |
| B2-6 | 32 | 1.796 | 1.1923 | 2.141 | 1.350 | 1.389 | 1.875 |
| B2-7 | 47 | 1.500 | 1.192 | 1.788 | 1.120 | 1.314 | 1.470 |
| B2-8 | 35.2 | 1.270 | 1.154 | 1.466 | 1.100 | 1.209 | 1.330 |

**Fig. 12.** Ductility Indexes from $P-\theta$ and $P-\Delta$ diagrams

shown in Fig. 12.

4.8 Energy Dissipation Capacity

The CPPF specimens absorbed energy by plastic deformation and underwent residual deformations after unloading with the descending branch of load-deflection curve. The plastic tube sealed and bridged the micro-cracks and exhibited a larger elongation at failure. The toughness of tube prevented crack initiation and propagation of cracks through the tube wall. The CPPF composite system increased the total energy absorbed, manifested itself by the large areas under the load-deflection curve i.e., ductility measured in terms of toughness increased, between 3 to 21 folds which is very important for the structural behavior in regions susceptible to earthquakes, and needs to be further researched. Unlike the PPF, the release of elastic energy for pure concrete was devastating. A concrete-encased by the PPF would have the durability and deformations of the tube but the mechanical strength and the rigidity of concrete.

4.9 Analytical

To quantify the composite action among the specimen components, the individual contributions from the unconfined concrete (P_C), steel reinforcement (P_S), plastic tube (P_{PPF}) in carrying the applied load, were analytically determined and superimposed for the three reinforcement systems. The superimposed relationships were as follows:

For CPPF only:

$$P_u = P_c + P_{PPF} = f'_c(A_c) + f'_{yPPF} \cdot A_{PPF} \quad (11)$$

Where,

A_C = cross-sectional area of concrete

A_{PPF} = area of PPF and was calculated from Eq. (12)

f'_c = the concrete compressive strength

f'_{yPPF} = compressive yield strength of tube

P_{PPF} = axial load resisted by the PPF

P_u = the maximum strength of equivalent short column

$$A_{PPF} = \frac{\pi}{4}(D_1^2 - D_2^2) \quad (12)$$

where D_1^2 and D_2^2 : the external and internal diameters of the tube, respectively. Although the CPPF specimen (B2-4) had single rebar ($1\phi 6$ mm deformed) in the centre of cross-section (Table 5), the rebar contribution was ignored since ($\rho_s = 0.0064$) < 0.01 as according to ACI 318-14.

For CPPF-SC column:

$$P_u = [P_C + P_S + P_{PPF}] \quad (13)$$

$$P_S = f'_y \cdot A_s \quad (14)$$

Where,

A_s = area of steel

f'_y = Steel yield strength

For CPPF-WM column:

$$P_u = [P_C + P_{WM} + P_{PPF}] \quad (15)$$

where P_{WM} : Axial load contribution of WM which was very small. For steel reinforced concrete column:

$$P_u = P_c + P_s = f'_c(A_c - A_s) + f'_y \cdot A_s \quad (16)$$

$$P_c = f'_c(A_c) \quad (17)$$

The steel-reinforced specimens (A1-3, A1-4, A1-6, A1-8) suffered considerable damage under the applied load. For most of the circular reinforced concrete columns, the longitudinal reinforcements attained yielding at the load which initiated the spalling of the concrete cover (Kim et al., 2007). Based on this assumption, all the tested reinforced specimens had reached the yield load. The two parameters which most influenced the capacity of the columns under the applied load were length effect and the rotation of upper loading platen. The load capacity of the tested slender column was evaluated as follows:

$$P_{Cal} = \Phi \cdot P_u \quad (18)$$

Where,

P_{cal} = the predicted load-bearing capacity of the slender column

P_u = the maximum strength of equivalent short column

Φ = buckling reduction factor

The slenderness ratio has a considerable influence on the buckling reduction factor. For CPPF columns, a buckling reduction factor, previously validated against 35 test results and proposed by (Yang et al., 2015), was used and is given by:

$$\Phi = 1 - 0.005\lambda \tag{19}$$

where λ : the slenderness ratio of the column ($0.8 l_u/r$). Eq. (19) underestimated the capacity of all columns and was calibrated using the current test results and was modified to:

$$\Phi = 1 - 0.006\lambda \tag{20}$$

All the predicted values and P_{Ex}/P_{Cal} ratios were summarized in Table 8, where P_{Ex}/P_{Cal18} , P_{Ex}/P_{Cal19} , P_{Ex}/P_{Cal20} represented the ratio of experimental to calculated load without reduction factor Eq. (18), and with reduction factor using Eqs. (19) and (20), respectively. A better prediction of P_{cal} and higher P_{Ex}/P_{Cal} ratio was obtained using Eq. (20). The difference between Eqs. (19) and (20) predictions may be ascribed to the loading platen (rotation effect). In addition to the length effect, the rotation of swiveling head resulted in the reduction in strength capacity too, especially for PC specimens which showed much lower strength due to its low resistance to non-axial stresses resulted from the upper loading platen rotation. The influence of PPF and composite action in improving the compressive and deformability performance of CPPF was present for the considered slenderness range.

Table 8. Experimental and Predicted Strength of Group A and B Columns

| No. | P_{Ex} (KN) | P_{cal18} (KN) | P_{Ex}/P_{cal18} | P_{cal19} (KN) | P_{Ex}/P_{cal19} | P_{cal20} (KN) | P_{Ex}/P_{cal20} |
|------|------------------|---------------------|--------------------|---------------------|--------------------|---------------------|--------------------|
| A1-1 | 72.00 | 120.50 | 0.60 | 95.80 | 0.75 | 90.86 | 0.79 |
| A1-2 | 56.50 | 120.50 | 0.47 | 92.79 | 0.61 | 87.24 | 0.65 |
| A1-3 | 212.0 | 311.92 | 0.68 | 252.7 | 0.84 | 240.8 | 0.88 |
| A1-4 | 230.4 | 311.92 | 0.74 | 262.0 | 0.88 | 252.0 | 0.91 |
| A1-5 | 86.50 | 157.40 | 0.55 | 122.8 | 0.71 | 115.8 | 0.75 |
| A1-6 | 218.0 | 311.92 | 0.70 | 257.3 | 0.85 | 246.4 | 0.89 |
| A1-7 | 74.00 | 120.50 | 0.61 | 97.00 | 0.76 | 92.30 | 0.80 |
| A1-8 | 216.0 | 318.68 | 0.68 | 258.1 | 0.84 | 246.0 | 0.88 |
| B2-1 | 294.2 | 385.51 | 0.76 | 318.05 | 0.93 | 304.55 | 0.97 |
| B2-2 | 147.8 | 245.93 | 0.60 | 201.89 | 0.73 | 194.28 | 0.76 |
| B2-3 | 155.4 | 245.93 | 0.63 | 206.58 | 0.75 | 198.71 | 0.78 |
| B2-4 | 107.0 | 158.67 | 0.67 | 124.56 | 0.86 | 117.73 | 0.91 |
| B2-5 | 119.5 | 170.79 | 0.70 | 134.07 | 0.89 | 126.73 | 0.94 |
| B2-6 | 221.66 | 312.70 | 0.71 | 262.67 | 0.84 | 252.66 | 0.88 |
| B2-7 | 93.00 | 144.75 | 0.64 | 113.63 | 0.82 | 107.40 | 0.87 |
| B2-8 | 184.0 | 262.67 | 0.70 | 216.44 | 0.85 | 207.19 | 0.89 |

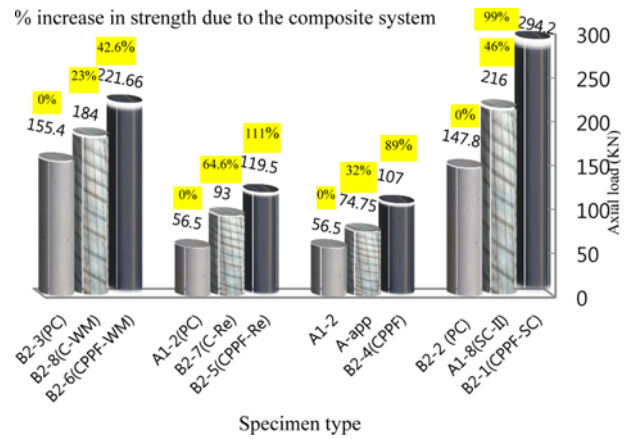


Fig. 13. Strength Capacity of Each Composite System and Its Equivalent RC and PC Strengths

4.10 Strength

The nominal strength increase in the post-yield range for CPPF was not substantial but it may be sufficient when a modest improvement in strength was desired. Approximately the load resisted by the CPPF with ($A_{PPF}/A_C = 24\%$) was equal to the load resistance of concrete specimen reinforced with $1\phi 6$ mm deformed rebar ($\rho_s = 0.0064 < 0.01$). Shear was adequately transferred between the concrete and PPF and spalling of concrete cover at high displacement was avoided. The compressive yield strength of the tube was only 40.5 MPa, nearly 12% of the yield strength of longitudinal steel bars (460 MPa). For the comparison purpose, no external metal edge protections were used in RC specimens. Thus, a stress concentration field due to the applied load appeared at the top end of the specimen and a fragile break in this area was not avoidable.

A comparison of the strength capacity of each composite system and its equivalent RC and PC strengths were shown in Fig. 13. For column (A1-8) with type II steel cage, the steel reinforcement increased the strength capacity of the column by 46% compared with its equivalent PC specimen (B2-2). With the inclusion of PPF the strength capacity of the column, CPPF-SC (B2-1), was increased by 36% over that of the reinforced column (A1-8) and by 99% over its equivalent PC specimen (B2-2). When compared with its equivalent specimen (A1-3) with steel cage type SC-I, the strength of CPPF-SC (B2-1) was 39% higher. A similar observation was made for the other two composite systems. Generally, the PPF resulted in strength increase of 36%, 43% for CPPF-SC (B2-1), CPPF (B2-4), compared with its equivalent steel-reinforced columns without PPF which had a smaller diameter (minus the thickness of tube). The other two composite columns, CPPF-Re (B2-5) and CPPF-WM (B2-6), yielded 28% and 20.5% increase in strength compared with its equivalent columns, B2-7 and B2-8, but with a similar diameter (all four had a diameter of 75mm). Column A-app (Table 5) was not cast and its ultimate experimental strength was approximated from its equivalent PC (A1-2) and CPPF (B2-4) for comparison purpose, Fig. 13.

5. Conclusions

The technical merit of using the PPF to encase and improve the deformation capacity of the concrete was investigated and the following conclusions were drawn:

1. The composite systems offered different rigidities which can ameliorate the axial and to less extent the radial performance of the specimen.
2. Slenderness ratio and rotation of the loading platen were the two main factors affecting the load-carrying capacity of the specimens.
3. The PPF improved the deformation of concrete due to the compression softening behavior. The maximum sustainable lateral displacement was increased several folds.
4. The B/A ratios were used to express the plastic rotation capacity of the columns. The CPPF specimens showed the highest B/A ratio 7.5 to 8.5 from the load-deflection curve and 6.67 to 8.3 from the load-rotation curve, whereas RC specimens showed lower values 1.55 to 2.54 and 1.72 to 1.88. The rotation capacity of PC specimens was negligible.
5. The three low-cost composite systems showed better results for the two ductility indexes, compared with its equivalent RC and PC specimens. The I_{c_s} and I_{c_d} values were 1.566 to 2.334 and 1.56 to 1.875 compared with 1.284 to 1.433 and 1.35 to 1.589 for its equivalent RC specimens.
6. The strength capacity of CPPF specimens was increased by 36%, 43%, 28%, and 20.5% compared with its equivalent steel reinforced columns without PPF.

The PPF is a new class of construction materials which can be used in infrastructure applications such as piers and bridge columns, due to its several advantages such as reducing the brittleness of concrete and providing additional shear and compressive capacity. The short-term structural feasibility of a promising material under axial load was examined. Long term performance is one of the several issues of concern for future research including fire and creep.

ORCID

Nwzad Abduljabar Abdulla  <https://orcid.org/0000-0001-5875-4321>

References

- Abdel Havez A (2014) Behavior of PVC encased reinforced concrete walls under eccentric axial loading. MSc Thesis, University of Waterloo, ON, Canada
- Abdulla NA (2014) Concrete filled thermoplastic tube under compression. Proceedings of 1st international engineering conference on developments in civil and computer engineering applications, November 24, University of Ishik, Erbil, Iraq, 60-70
- Abdulla NA (2017) Concrete filled PVC tube: A review. *Construction and Building Materials* 156:321-9, DOI: 10.1016/j.conbuildmat.2017.08.156
- Abdulla NA (2019) Influence of plastic pour-in form on mechanical behavior of concrete. *Structures* 19:193-202, DOI: 10.1016/j.istruc.2019.01.007
- ACI 318R-14 (2014) Requirements for structural concrete. ACI 318R-14, American Concrete Institute, Farmington Hills, MI, USA
- ACI 440 2R-08 (2008) Guide for the design and construction of externally bonded FRP systems for strengthening concrete structures. ACI 440 2R-08, American Concrete Institute, Farmington Hills, MI, USA
- ASCE/SEI-41 (2007) Seismic rehabilitation of existing structures. ASCE/SEI Committee 41, ASCE Standard, Reston, VA, USA
- Chen Y, Feng R, Xiong L (2016) Experimental and numerical investigations on steel-concrete-PVC SHS joints under axial compression. *Construction and Building Materials* 102:654-670, DOI: 10.1016/j.conbuildmat.2015.11.013
- Ding L, Seliem HM, Rizkalla SH, Wu G, Wu Z (2011) Behavior of concrete piles confined with CFRP grid fiber-reinforced polymer reinforcement for concrete structures. 10th international symposium, April 2-4, Tampa, FL, USA
- Fakharifar M, Chen G (2016) Compressive behavior of FRP-confined concrete-filled PVC tubular columns. *Composite Structures* 141:91-109, DOI: 10.1016/j.compstruct.2016.01.004
- Fujiwara Y, Maruya T, Owaki E (1992) Degradation of concrete buried in soil with saline groundwater. *Nuclear Engineering* 138(2):143-150
- Ghannoum WM, Matamoros AB (2014) Nonlinear modeling parameters and acceptance criteria for concrete columns. *ACI Special Publication* 297:1-24
- Kim TH, Kim YJ, Kang HT, Shin HM (2007) Performance assessment of reinforced concrete bridge columns using a damage index. *Canadian Journal of Civil Engineering* 34(7):843-855, DOI: 10.1139/07-003
- Lima Junior HC, Giongo JS (2004) Steel fiber high strength concrete prisms confined by rectangular ties under concentric compression. *Journal of Materials and Structures* 37:689-697, DOI: 10.1007/BF02480514
- Maiturare FD (1990) Strength of Concrete Column Confined by Plastic Pipe. MSc Thesis, Ahmadu Bello University, Zaria, Nigeria
- Merah N, Bazoune A, Khan Z (2013) Artificial and natural weathering of chlorinated polyvinyl chloride (CPVC). *Advanced Materials Research* 652-654:1277-1282, DOI: 10.4028/www.scientific.net/AMR.652-654.1277
- Mufti AA, New hook JP, Tadros G (1996) Deformability versus ductility in concrete beams with FRP reinforcement. Proceedings of the 2nd International conference on advanced composite materials in bridges and structures, August 11-14, Montreal, Canada, 189-199
- Naish D, Nguyen J, Jimenez O, Hoenisch B (2013) Experimental assessment of the effect of PVC attachments as repair of RC beams. *Journal of Civil Engineering and Architecture* 1(4):114-119, DOI: 10.13189/cea.2013.010403
- Oyawa WO, Gathimba WO, Mang'uriu GN (2016) Structural response of composite concrete-filled plastic tubes in compression. *Steel and Composite Structures* 21(3):589-604, DOI: 10.12989/scs.2016.21.3.589
- Pan M, Shi X, Li X, Hu H, Zhang L (2004) Morphology and properties of PVC/clay nanocomposites via in situ emulsion polymerization. *Journal of Applied Polymer Science* 94(1):277-286, DOI: 10.1002/app.20896
- Sezen H, Moehle JP (2004) Shear strength model for lightly reinforced concrete columns. *Journal of Structural Engineering* 130(11):1692-1703, DOI: 10.1061/(ASCE)0733-445(2004)130:11(1692)

- Sheikh SA, Uzumeri SM (1982) Analytical model for concrete confinement in tied columns. *Journal of the Structural Division* 108(ST12):2703-2722
- Stapleman J (1997) Pile on the abuse. *Composite Technology*
- United States Department of Transportation (2006) A laboratory and field study of composite piles for bridge substructures. FHWA-HRT-04-043, Office of Research, Development and Technology, Charlottesville, VA, USA
- Xiamuxi A, Hasegawa A (2011) Experimental study on the reinforcement ratio of RCFT columns under axial compression. *Advanced Materials Research* 250-253:3790-3797, DOI: [10.4028/www.scientific.net/AMR.250-253.3790](https://doi.org/10.4028/www.scientific.net/AMR.250-253.3790)
- Yang H, Liu FQ, Gardner L (2015) Post-fire behavior of slender reinforced concrete columns confined by circular steel tubes. *Thin-Walled Structures* 87:12-29